RSC Advances

PAPER

View Article Online
View Journal | View Issue

Cite this: *RSC Adv.*, 2017, **7**, 16282

Towards high visible light photocatalytic activity in rare earth and N co-doped $SrTiO_3$: a first principles evaluation and prediction

Chao Zhang,*[a] Nan Jiang,[a] Shiai Xu,[ab] Zheng Li,[a] Xingliang Liu,[a] Tianle Cheng,[a] Aixia Han,[a] Haitang Lv,[a] Wenliang Sun[a] and Yunlei Hou[a]

Received 6th December 2016
Accepted 2nd March 2017

DOI: 10.1039/c6ra27840j

rsc.li/rsc-advances

The band structure and photocatalytic activity of RE (La, Ce, Pr or Nd) mono-doped and RE–N co-doped $SrTiO_3$ for band gap reduction are studied systematically using first principles calculations. Based on the evaluation methods proposed by us previously, various RE–N co-doped cases with La–N, Ce–N, Pr–N and Nd–N co-doped in $SrTiO_3$ are studied. By comprehensive comparison, the favourable co-doping dopants are obtained and the predicted Pr–N co-doped $SrTiO_3$ shows that it may serve as an effective potential candidate photocatalyst for water splitting under visible light among the four types of RE–N co-doped cases. In addition, the f state electrons from the RE atom may have a greater contribution to the band structure narrowing of the RE–N co-doped $SrTiO_3$.

1. Introduction

Currently, there are numerous studies on exploiting the potential of semiconductor-based photocatalysts for water splitting and hydrogen production.[1,2] As one of the typical perovskites, $SrTiO_3$ has been extensively studied for its potential application in this area.[3–5] However, due to the wide band gap (about 3.2 eV) of $SrTiO_3$, it shows a poor response on its exposure to visible light.[6] Currently, several researchers are trying to obtain substantially more sunlight by narrowing the band gap of $SrTiO_3$. A common strategy for band gap reduction is to dope $SrTiO_3$ structures with various cations or anions.[7–11] Since mono-doping may cause compensating defects, co-doping has been proposed to overcome these limitations in $SrTiO_3$.[12–17]

There have been numerous reports on transition metal ion or noble metal dopants with non-metal co-doping on $SrTiO_3$ previously. However, the rare-earth with non-metal co-doped $SrTiO_3$ and their photocatalytic properties have seldom been reported thus far. Only a few research studies mention this topic. Wei *et al.*[18] reported that the donor–acceptor pair recombination by co-doping could maintain the charge balance and promote the photogenerated carriers efficiency for N–La co-doped $SrTiO_3$ under visible light. Wang *et al.*[19] reported co-doping (N–La, C–Ce, and N–Ce–N) on the electronic structure of $SrTiO_3$ and found that (N–Ce–N) co-doping can significantly narrow the band gap of $SrTiO_3$. Dawson *et al.*[20] reported the defect chemistry of RE mono-doped $SrTiO_3$/$CaTiO_3$/$BaTiO_3$ and found that RE doping is energetically preferred in $BaTiO_3$ and least favourable in $SrTiO_3$.

Recently, the rare earths have attracted great attention with TiO_2 and have shown their importance in the TiO_2 matrix due to their incompletely occupied 4f and empty 5d states.[21] The photocatalytic activity of TiO_2 is improved by rare earth (RE) doping and the high oxidation states of RE ions may serve as efficient electron traps.[22–25] Inspired by this, we think that it is necessary to systematically study the electronic structure and band edge of $SrTiO_3$ doped with RE elements or co-doped with RE and non-metals. In addition, since the RE elements have similar ionic radii and complex 4f or 5d electrons, it is a great challenge to accurately calculate their electronic structure and predict the best co-doping properties.

Herein, we present a comparative study on the electronic structure and photocatalytic activity of RE and N co-doped $SrTiO_3$ with RE (La, Ce, Pr or Nd) as a donor and N as an acceptor for band gap reduction. By combining the evaluation methods proposed by us previously,[26] we pick the best co-doping dopant among the listed four co-doped cases *via* systematic evaluation and prediction. Moreover, the band structure of the chosen Pr–N co-doped $SrTiO_3$ shows that it may be a good candidate photocatalyst for water splitting under visible light.

2. Computational methods

Herein, all the calculations carried out were performed *via* density functional theory (DFT) using the CASTEP code.[27] The PBE function within GGA was used. The valence electrons and

[a]*Chemical Engineering College, Qinghai University, Xining 810016, China. E-mail: zhangchaoqhu@126.com; Fax: +86-971-5310427; Tel: +86-971-5310427*

[b]*Shanghai Key Laboratory of Advanced Polymeric Materials, Key Laboratory for Ultrafine Materials of Ministry of Education, School of Materials Science and Engineering, East China University of Science and Technology, Shanghai 200237, China*

ionic core interaction were calculated by the Perdew–Wang 91 gradient-corrected functional[28] and ultra-soft pseudo-potentials.[29] The cut-off energy (E_{cut}) was set at 390 eV and a 2 × 2 × 2 Monkhorst–Pack[30] k-mesh was adopted. The energy convergence was set to 5×10^{-5} eV per atom. The largest force on atoms was set at 0.1 eV Å^{-1} for convergence and criterion optimization. The stress was less than 0.2 GPa, and the maximum displacement was 5×10^{-4} nm. For the doping cases, a 2 × 2 × 2 $SrTiO_3$ supercell with 40 atoms was used. N atom for O atom and RE (La, Ce, Pr or Nd) atom for Sr atom substitution was used in the $SrTiO_3$ structure to model the N or RE mono-doping case. In the case of co-doping, we introduced both N and RE atoms in the $SrTiO_3$ crystal structure with an N atom for O and RE atom for Sr in the same super structure to model the La–N, Ce–N, Pr–N and Nd–N co-doping. The chosen valence electronic configurations were 4s, 4p and 5s for Sr, 4s and 3d for Ti, 2s and 2p for O, 2s and 2p for N, 5s, 5p, 5d and 6s for La, 4f1, 5s2, 5p6, 5d1 and 6s2 for Ce, 4f3, 5s2, 5p6 and 6s2 for Pr, and 4f4, 5s2, 5p6 and 6s2 for Nd. The DFT + U formalism[31,32] was employed for the accurate treatment of the correlated f or d electron phenomena with $U = 6.0$ eV.[28]

3. Results and discussion

3.1. RE mono-doping in $SrTiO_3$

3.1.1. RE mono-doping effects on formation energy and lattice parameters of $SrTiO_3$. The calculated structure of the un-doped $SrTiO_3$ crystal was determined first. The optimized structural parameters of the pure $SrTiO_3$ ($a = b = c = 3.935$ Å) are in good agreement with the experimental data[33] ($a = b = c = 3.905$ Å). For RE mono-doping on $SrTiO_3$, La prefers to substitute for the Sr site and because the ionic radii of Ce^{3+} (0.103 nm), Pr^{3+} (0.101 nm) and Nd^{3+} (0.100 nm) are similar to La^{3+} (0.115 nm), herein, we mainly consider the RE (La, Ce, Pr or Nd) atom substitute for the Sr site, which is described as La@Sr, Ce@Sr, Pr@Sr and Nd@Sr mono-doped $SrTiO_3$, respectively. All of the RE atom mono-doped models are labelled in Fig. 1(b).

In order to obtain the formation energy needed for the different mono doped cases, the doping formation energy (E_f) of the different mono-doped cases was calculated according to the listed formulas and the results are shown in Table 1.

Table 1 The calculated formation energies (E_f), and band gaps (E_g) of the different RE dopant mono-doped $SrTiO_3$

Dopant	E_f (eV)	E_g (eV)	E_g with scissor operator (1.0 eV)
Pure	—	2.20	3.20
La@Sr	−0.25	1.45	2.45
Ce@Sr	−1.17	2.36	3.36
Pr@Sr	−1.16	1.94	2.94
Nd@Sr	−1.04	1.11	2.11

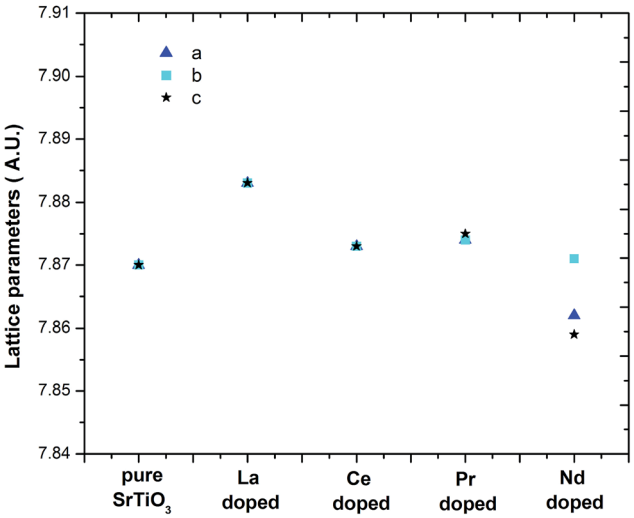

Fig. 2 Lattice parameters (supercell) change with the different types of RE mono-doped $SrTiO_3$.

$$E_f = E_{N\text{-doped}} - (E_{un\text{-doped}} - \mu_O + \mu_N) \quad (1)$$

$$E_f = E_{La(Ce/Pr/Nd)\text{-doped}} - [E_{un\text{-doped}} - \mu_{Sr} + \mu_{La} \text{ (or } \mu_{Ce}/\mu_{Pr}/\mu_{Nd})] \quad (2)$$

The E_f defines the energy of the mono or co-doped dopants in $SrTiO_3$, and $E_{un\text{-doped}}$, $E_{N\text{-doped}}$, $E_{La\text{-doped}}$, $E_{Ce\text{-doped}}$, $E_{Pr\text{-doped}}$, $E_{Nd\text{-doped}}$, are the total energies of the $SrTiO_3$ without doping and with N doping, La doping, Ce doping, Pr doping, and Nd

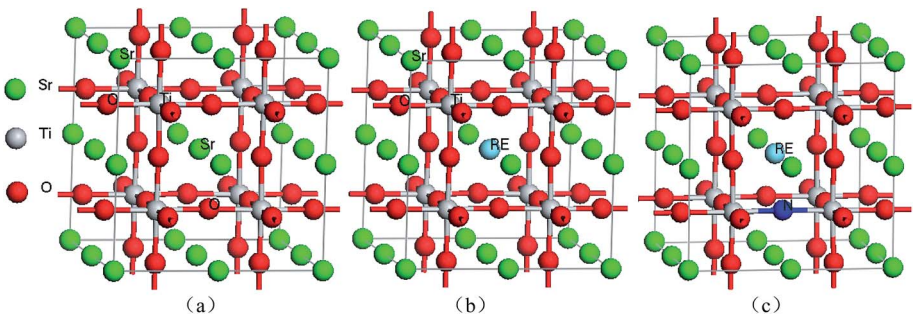

Fig. 1 $SrTiO_3$ supercell models (a) un-doped 2 × 2 × 2 $SrTiO_3$ supercell, (b) one RE atom mono-doped 2 × 2 × 2 $SrTiO_3$ supercell, and (c) RE–N co-doped 2 × 2 × 2 $SrTiO_3$ supercell (RE = La, Ce, Pr or Nd atom); green, light gray, and red balls represent Sr, Ti, and O atoms, respectively.

doping, respectively. μ_O and μ_N are the energies of the O and N atom gained from the energies of the O_2 and N_2 molecular orbitals, respectively. μ_{Sr}, μ_{Ti}, μ_{La}, μ_{Ce}, μ_{Pr} and μ_{Nd} are calculated from the bulk Sr (gamma-strontium),[34] Ti (alpha-titanium),[35] La (hcp, structure),[36] Ce (hcp, structure),[36] Pr (hcp, structure),[36] and Nd (hcp, structure) crystals, respectively.

The smaller the defect formation energy needed, the more favourable the substitution for the dopant. From Table 1, the result shows that the formation energy of La@Sr is −0.25 eV, which is much larger than that of Ce@Sr, Pr@Sr or Nd@Sr. This is reasonable since the ionic radius of La^{3+} (0.115 nm) is larger than that of Ce^{3+} (0.103 nm), Pr^{3+} (0.101 nm) or Nd^{3+} (0.100 nm),

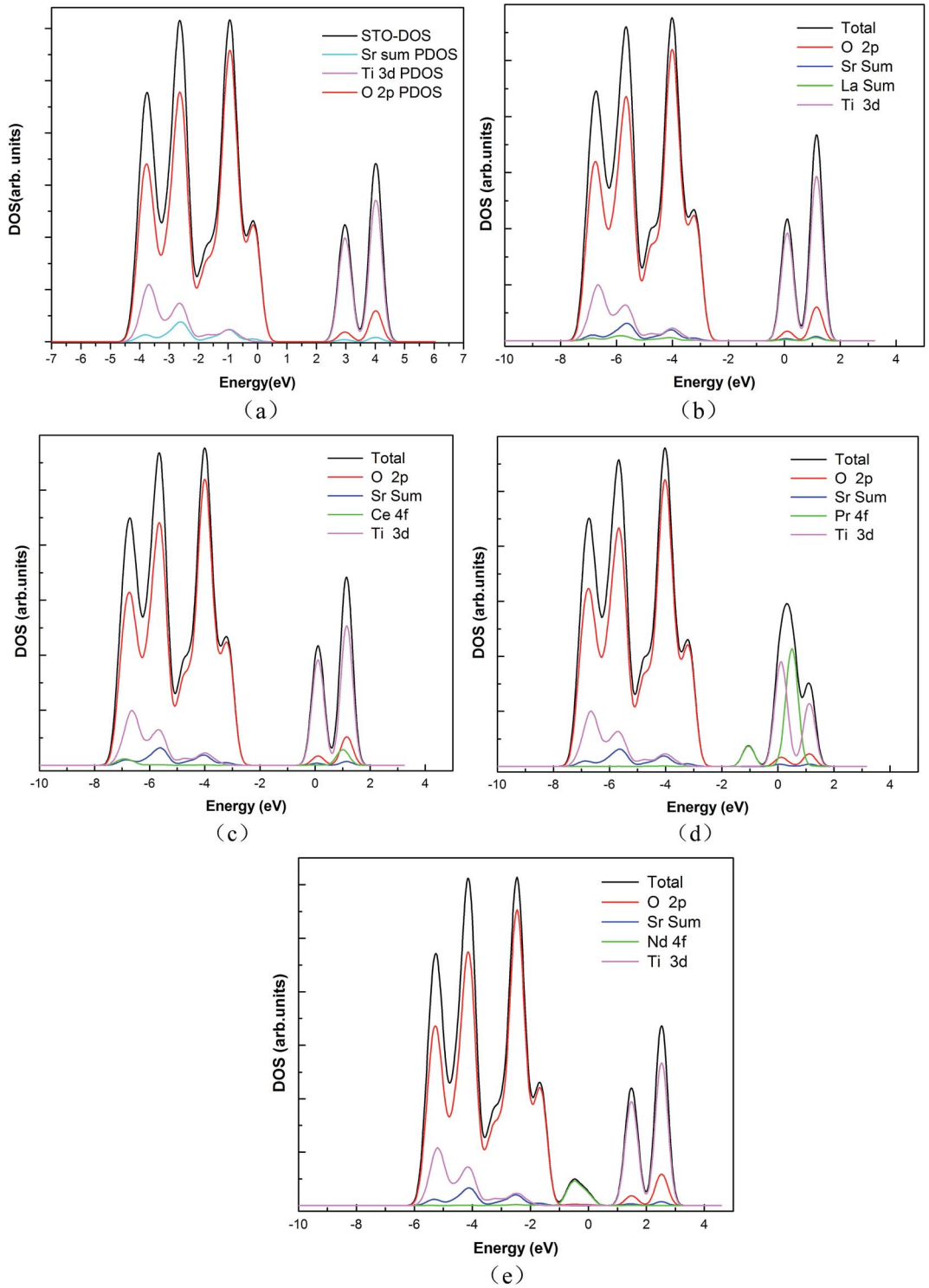

Fig. 3 Calculated DOS for (a) pure $SrTiO_3$, (b) substitutional La for Sr doped $SrTiO_3$, (c) substitutional Ce for Sr doped $SrTiO_3$, (d) substitutional Pr for Sr doped $SrTiO_3$, and (e) substitutional Nd for Sr doped $SrTiO_3$. The VBM of pure $SrTiO_3$ is chosen as the energy zero.

which leads to the relative larger formation energy of Sr substituted by La.

The calculated lattice parameters (supercell) of the different RE mono-doped $SrTiO_3$ are shown in Fig. 2. From the lattice parameters trend we may conclude that La is energetically unfavourable compared with the Ce, Pr or Nd mono-doped cases, which is consistent with the changing trend of the defect formation energy or ionic radius of the four different RE mono-doped $SrTiO_3$.

3.1.2. RE mono-doping on band structure and band gap of $SrTiO_3$. The DOS and PDOS for pure and RE mono-doped $SrTiO_3$ calculated are shown in Fig. 3. It is clear that the VBM is mainly determined by the O 2p and Sr related states and the Ti 3d states mainly contribute to the CBM for un-doped $SrTiO_3$. For the substituted La@Sr, Ce@Sr, Pr@Sr and Nd@Sr mono-doped $SrTiO_3$, the La@Sr mono-doped case has a relatively small effect on the band structure of $SrTiO_3$ (Fig. 3(b)), whereas the other three cases have a relatively big effect on the band structure of $SrTiO_3$. The 4f orbit electrons have a bigger contribution on the band structure narrowing of Pr or Nd mono-doped $SrTiO_3$. In addition, the f electron of Ce and Pr mainly located in the CB and the f electron of Nd tend to fall between the VB and CB of $SrTiO_3$, which may be due to the different f electron energies of the Ce, Pr and Nd atoms (Fig. 3(c and e)).

The band gap of the Pr@Sr or Nd@Sr mono-doped $SrTiO_3$ case shows some degree of narrowing, and in the Ce@Sr mono-doped case, it shows some degree of increase compared with the pure case (Table 1). From Table 1 we can clearly see that the band gap of La (Pr or Nd) mono-doped $SrTiO_3$ case shows some kind of narrowing, whereas in the Ce mono-doped $SrTiO_3$ case, it tends to slightly increase.

In order to describe the oxidation and reduction power of the RE mono-doped $SrTiO_3$, the valence band (VB) bottoms (E_{VB}) and conduction band (CB) bottoms (E_{CB}) were calculated empirically according to formula (3).[37] Moreover, the suitable band edge of the catalyst should lie between the water reduction and oxidation potential, which means that the conduction band edge should lie at a potential more negative than the water reduction potential (<0 V *vs.* NHE at pH 0).

$$E_{CB} = x_{A_aB_bC_c} - \frac{1}{2}E_g + E_0 \quad (3)$$

where E_g is the band gap, E_0 is the scale factor relating the reference electrode redox level to the absolute vacuum scale ($E_0 = -4.5$ eV for a normal hydrogen electrode), and $x_{A_aB_bC_c}$ is the absolute electronegativity of compound $A_aB_bC_c$, where the absolute electronegativity of La (Ce, Pr and Nd) atom was obtained from that reported by Bartolotti.[38]

The calculated E_{CB} of pure, La mono-doped, Ce mono-doped, Pr mono-doped and Nd mono-doped $SrTiO_3$ are −1.16, −0.73, −1.19, −0.95, and −0.52 eV, respectively. Thus, the VB tops are 2.04, 1.72, 2.17, 1.99 and 1.59 eV, respectively. From the calculated E_{CB} and E_{VB} in Fig. 4, we conclude that the four types of RE mono-doped $SrTiO_3$ meet the requirements for water reduction without considering their efficiency, where the La (Pr or Nd) mono-doped case may be the best choice.

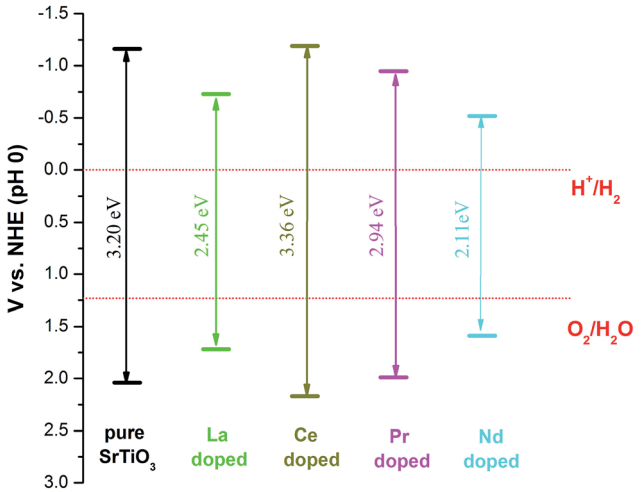

Fig. 4 Calculated E_{CB} and E_{VB} of RE mono-doped $SrTiO_3$ compared with the water reduction potential (<0 V *vs.* NHE at pH 0).

3.2. RE co-doping in $SrTiO_3$

3.2.1. RE co-doping effects on formation energy and lattice parameters of $SrTiO_3$. The formation energy needed for the different RE–N co-doped cases can be calculated similarly to that of the RE mono-doped cases, as previously described, with some revisions to the formula (formula (4)).

$$E_f = E_{La(Ce/Pr/Nd)\text{–}N\text{-co-doped}} - [E_{un\text{-}doped} - \mu_O - \mu_{Sr} + \mu_N + \mu_{La}(\text{or } \mu_{Ce}/\mu_{Pr}/\mu_{Nd})] \quad (4)$$

The calculated atomic structures of the different RE–N co-dopings on $SrTiO_3$ are shown in Fig. 1(c) and the lattice parameters (supercell) of the different RE–N co-doped $SrTiO_3$ are listed in Table 2.

From Table 2, it can be seen that the obtained formation energy of the La–N co-doped case is much larger than the other three Ce(Pr/Nd)–N co-doped cases. The change trend is similar to that of the RE mono-doped case.

For the RE–N co-doping cases, the binding energy should also be considered, which can describe the coupling strength of the RE–N co-doping cases. The defect pair binding energies were calculated according to the formula mentioned by Wei *et al.*[18] The obtained binding energies are 1.84 eV, 1.34 eV, 1.91 eV and 1.11 eV for La–N, Ce–N, Pr–N and Nd–N co-doped $SrTiO_3$. This, La–N and Pr–N may be more stable for $SrTiO_3$ co-doping just from this point of view.

Table 2 The RE–N co-doping formation energies (E_f), binding energies (E_b) and band gaps (E_g) of $SrTiO_3$

Dopant	E_f (eV)	E_b (eV)	E_g (eV)	E_g with scissor operator (1.0 eV)
Pure	—	—	2.20	3.20
La–N co-doped	8.27	1.84	1.02	2.02
Ce–N co-doped	3.36	1.34	1.01	2.01
Pr–N co-doped	2.49	1.91	0.99	1.99
Nd–N co-doped	3.35	1.11	0.23	1.23

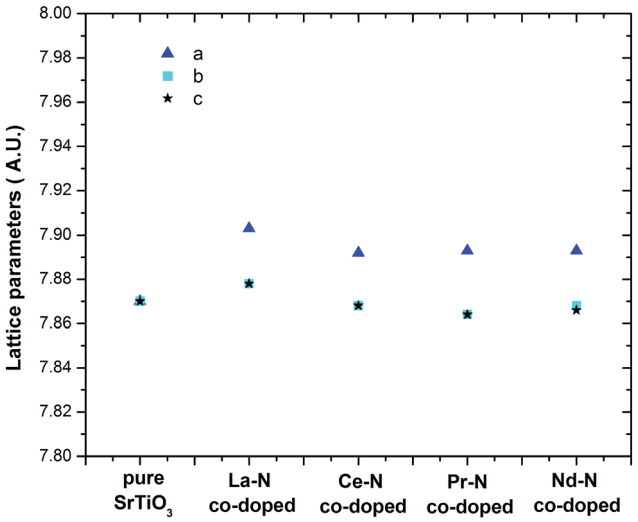

Fig. 5 Lattice parameter (supercell) changes with different types of RE–N co-doped $SrTiO_3$.

The lattice parameters (supercell) of the different RE–N co-doped $SrTiO_3$ were also calculated, and the result is shown in Fig. 5. From the calculated result it can be seen that the lattice parameter *a* has a larger change than that of *b* or *c*, which is different from that of the RE mono-doped cases. This type of difference mainly originates from the N substitution for the O site, which also means that this type of substitution is more difficult than the RE substitution for the Sr site.

3.2.2. RE–N co-doping effects on band structure and band gap of $SrTiO_3$. To get a better understanding of the electronic structure of the different RE–N co-doped cases of $SrTiO_3$, we calculated the electronic band structure of the La–N, Ce–N, Pr–N and Nd–N co-doped $SrTiO_3$. From the obtained band structure, it can be seen that the La–N, Ce–N and Pr–N co-doped $SrTiO_3$ tend to be a direct band gap semiconductor. In addition, no single donor or acceptor level appears between the VB and CB, which means that the electron of the donor level from the RE element (La/Ce/Pr or Nd) passivates the same amount of holes on the acceptor level from N (Fig. 6(a–c)).

We also calculated the total DOS and PDOS for the RE–N co-doped $SrTiO_3$, as shown in Fig. 7. From the PDOS of Ce or Pr–N co-doped $SrTiO_3$, we find that the N 2p states form an effective complementarity with that of the Ce or Pr 4f states, which can effectively reduce the band gap (shown in Fig. 7(c and d)). However, the band structure almost tends to have conductor character for the Nd–N co-doped case, which may be due to the fact that the energy of the complete 4f states just falls between the VB and CB of $SrTiO_3$ after the co-doping (shown in Fig. 7(d)).

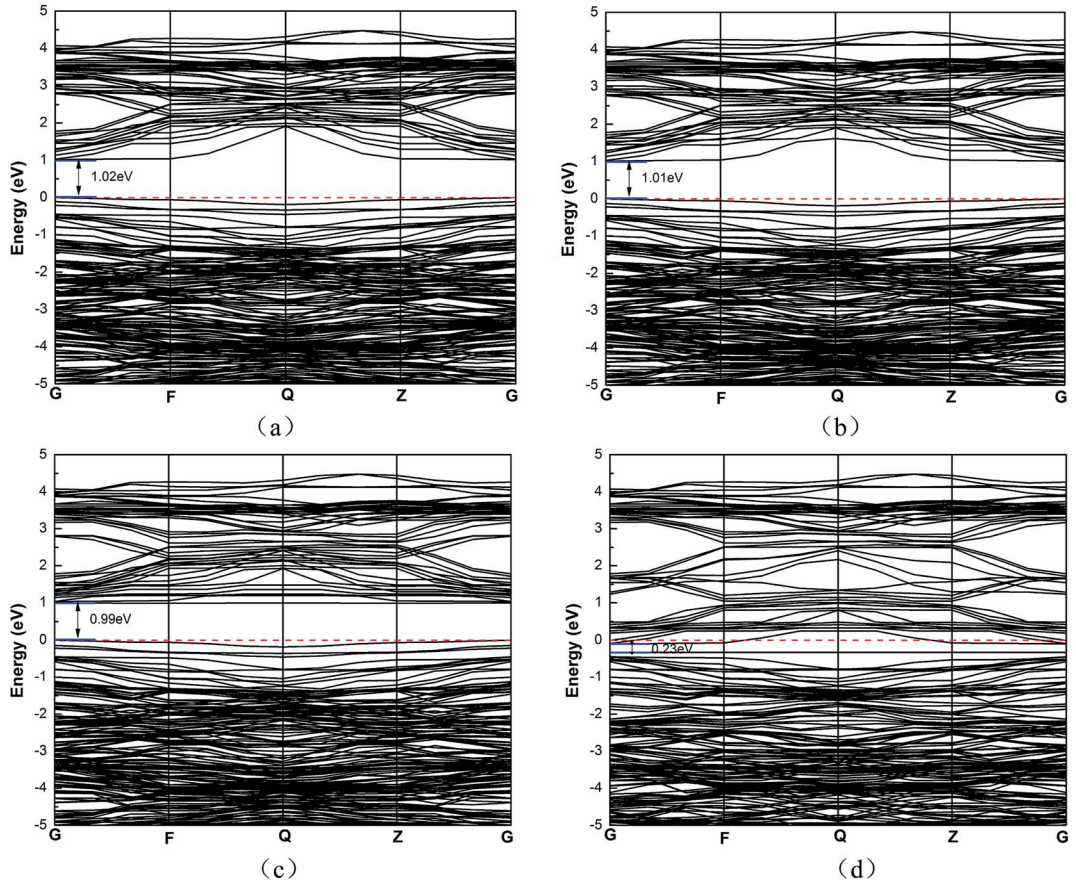

Fig. 6 Band structure plots of (a) La–N co-doped 2 × 2 × 2 $SrTiO_3$ super-cell, (b) Ce–N co-doped 2 × 2 × 2 $SrTiO_3$ super-cell, (c) Pr–N co-doped 2 × 2 × 2 $SrTiO_3$ super-cell and (d) Nd–N co-doped 2 × 2 × 2 $SrTiO_3$ super-cell.

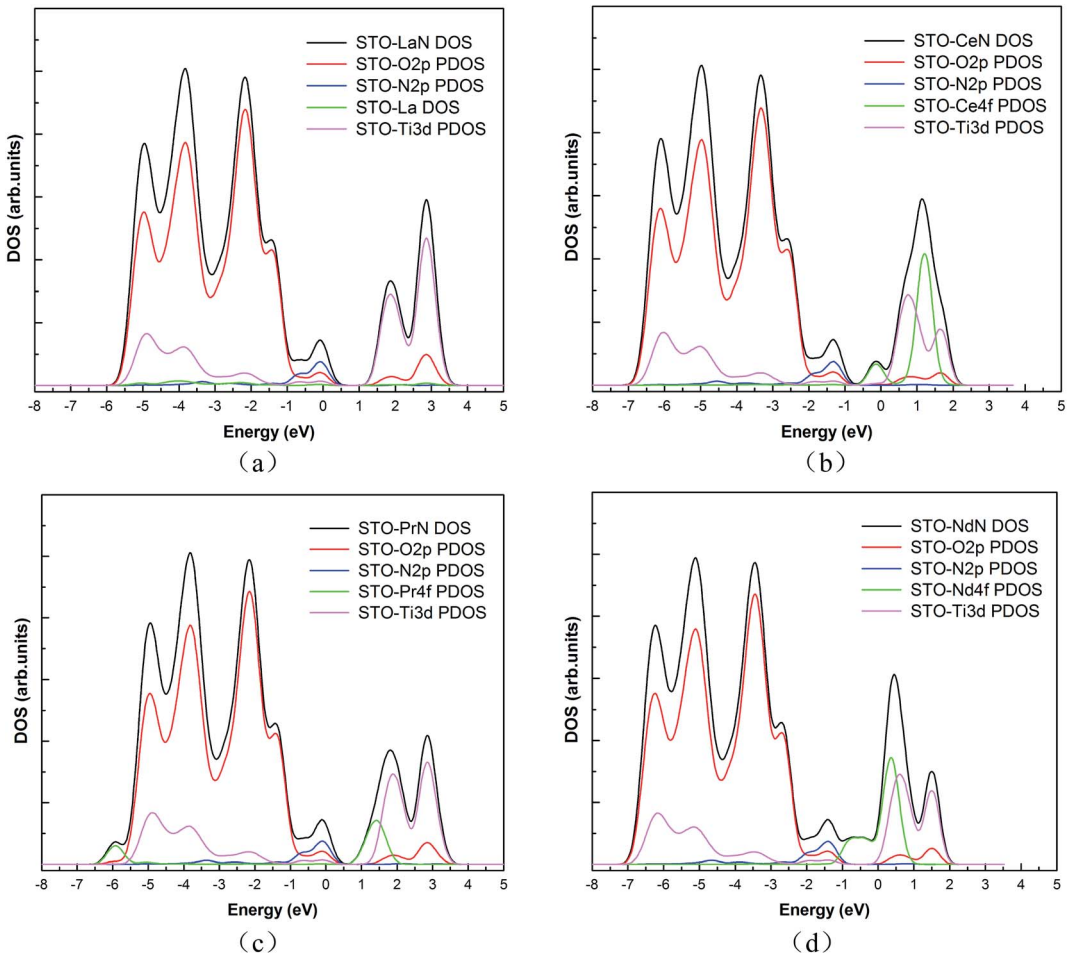

Fig. 7 Calculated DOS and PDOS for (a) La–N co-doped $SrTiO_3$, (b) Ce–N co-doped $SrTiO_3$, (c) Pr–N co-doped $SrTiO_3$, and (d) Nd–N co-doped $SrTiO_3$. The VBM of pure $SrTiO_3$ is chosen as the energy zero.

The band gap of the RE–N co-doped $SrTiO_3$ can be seen in Table 2. It is clear that the four types of RE–N co-doped $SrTiO_3$ cases all tend to have a narrowing trend compared with that of pure $SrTiO_3$, which is different from that of the RE mono-doped cases. This difference indicates that the RE–N co-doped cases may have a greater impact on the band gap compared with that of the RE mono-doped cases, and thus RE–N co-doping may be a better strategy.

It is difficult to select a suitable RE–N co-doping from the abovementioned four types of co-doping cases just from the value of the band gap; we also have to consider the precise band edge of the valence band (VB) bottoms (E_{VB}) and conduction band (CB) bottoms (E_{CB}) of the co-doped case. Thus, the E_{VB} and E_{CB} of the RE–N co-doped cases were calculated also using formula (3).

The calculated E_{CB} of the La–N co-doped, Ce–N co-doped, Pr–N co-doped and Nd–N co-doped $SrTiO_3$ were −0.52, −0.52, −0.48 and −0.08 eV, respectively, and thus the VB tops were 1.50, 1.49, 1.51 and 1.15 eV, respectively. The precise band edges of the E_{VB} and E_{CB} of La–N, Ce–N, Pr–N and Nd–N co-doped $SrTiO_3$ are shown in Fig. 8. From the obtained E_{CB} and E_{VB}, we could deduce that the band edges of La–N, Ce–N and Pr–N co-doped $SrTiO_3$ are located just out of the NHE potential and could well meet the requirements for water splitting and hydrogen production.

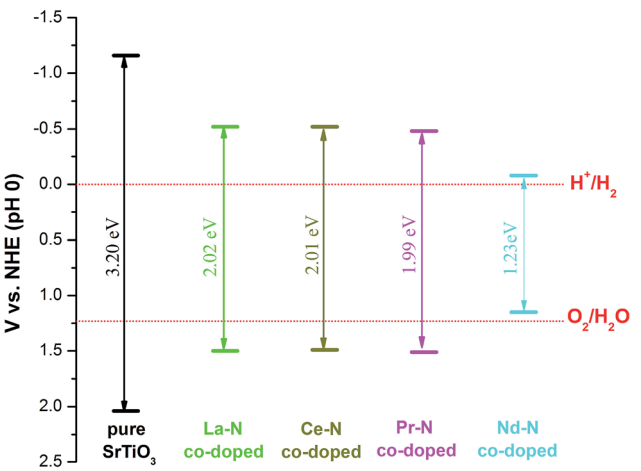

Fig. 8 The calculated E_{CB} and E_{VB} of the RE–N co-doped $SrTiO_3$ compared with the water reduction potential (<0 V *vs.* NHE at pH 0).

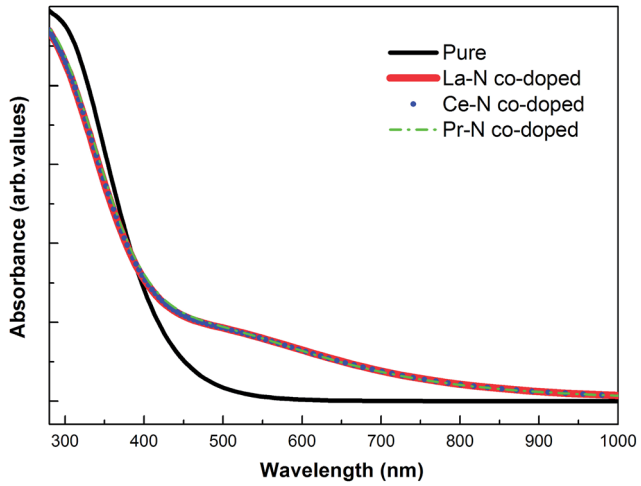

Fig. 9 Calculated optical absorption curves for pure, La–N, Ce–N, and Pr–N co-doped $SrTiO_3$.

3.2.3. Optical properties. The optical properties can be calculated from the dielectric function $\varepsilon(\omega) = \varepsilon_1(\omega) + i\varepsilon_2(\omega)$, and the imaginary part of the dielectric constant (ε_2) can be calculated theoretically based on DFT.[39] A rigid scissor operator correction of 1.0 eV was adopted for the absorption spectra calculation. Then, the optical absorption coefficients for La–N, Ce–N, Pr–N and Nd–N co-doped $SrTiO_3$ and pure $SrTiO_3$ were calculated, and the obtained results are listed in Fig. 9. From the calculated absorption data, it can be seen that the absorption edge tends to redshift compared with the un-doped case for the co-doping of La–N, Ce–N, and Pr–N.

3.3. Prediction and picking the favorable RE–N co-doping dopants on $SrTiO_3$

As described before, it is insufficient to predict one RE–N co-doping case from the given La–N, Ce–N, Pr–N or Nd–N co-doping systems as the best candidate. Based on the three basic rules proposed by us previously,[26] we choose the best co-doping dopant among the listed four co-doped cases *via* systematic evaluation and prediction. By comprehensively combining the band gap, the precise band edge of E_{VB} and E_{CB}, the formation energy and binding energy of the different RE–N co-doping cases, the Pr–N co-doped dopant may be a good potential candidate for the co-doping of $SrTiO_3$ among the La–N, Ce–N, Pr–N and Nd–N co-doped cases, which may serve as an effective potential candidate photocatalyst.

4. Conclusion

We present a comparative calculation on the electronic structure and photocatalytic of RE (La, Ce, Pr or Nd)–N co-doped $SrTiO_3$ for band gap reduction. Based on the evaluation methods proposed by us previously, various types of RE–N co-doping cases with La–N, Ce–N, Pr–N and Nd–N co-doped in $SrTiO_3$ are studied. The obtained favourable co-doping dopant and the predicted Pr–N co-doped $SrTiO_3$ shows that it may serve as an effective potential candidate photocatalyst for water splitting under visible light among the four RE co-doped cases. In addition, the f state electrons from the RE atom may have a greater contribution to the band structure narrowing of the RE–N co-doped $SrTiO_3$.

Acknowledgements

This study is financially supported by the Natural Science Foundation of QingHai Science & Technology Department (2016-ZJ-946Q). The Computer Network Information Center (CNIC) is also acknowledged for high-performance computing services.

References

1 B. Modak, K. Srinivasu and S. K. Ghosh, Improving photocatalytic properties of $SrTiO_3$ through (Sb, N) codoping: a hybrid density functional study, *RSC Adv.*, 2014, **4**(86), 45703–45709.
2 X. Chen, S. Shen, L. Guo and S. S. Mao, Semiconductor-based photocatalytic hydrogen generation, *Chem. Rev.*, 2010, **110**(11), 6503–6570.
3 P. Reunchan, S. Ouyang, N. Umezawa, H. Xu, Y. Zhang and J. Ye, Theoretical design of highly active $SrTiO_3$-based photocatalysts by a codoping scheme towards solar energy utilization for hydrogen production, *J. Mater. Chem. A*, 2013, **1**, 4221–4227.
4 S. Hara, M. Yoshimizu, S. Tanigawa, L. Ni, B. Ohtani and H. Irie, Hydrogen and oxygen evolution photocatalysts synthesized from strontium titanate by controlled doping and their performance in two-step overall water splitting under visible light, *J. Phys. Chem. C*, 2012, **116**, 17458–17463.
5 Q. Fu, T. He, J. L. Li and G. W. Yang, Band-engineered $SrTiO_3$ nanowires for visible light photocatalysis, *J. Appl. Phys.*, 2013, **113**, 104303.
6 M. Batzill, E. H. Morales and U. Diebold, Influence of nitrogen doping on the defect formation and surface properties of TiO_2 rutile and anatase, *Phys. Rev. Lett.*, 2006, **96**, 26103.
7 W. Wei, Y. Dai, H. Jin and B. B. Huang, Density functional characterization of the electronic structure and optical properties of Cr-doped $SrTiO_3$, *J. Phys. D: Appl. Phys.*, 2009, **42**, 055401.
8 H. Irie, Y. Maruyama and K. Hashimoto, Ag^+- and Pb^{2+}-Doped $SrTiO_3$ Photocatalysts: A correlation Between Band Structure and Photocatalytic Activity, *J. Phys. Chem. C*, 1847, **2007**, 111.
9 R. Konta, T. Ishii, H. Kato and A. Kudo, Photocatalytic activities of noble metal ion doped $SrTiO_3$ under visible light irradiation, *J. Phys. Chem. B*, 2004, **108**, 8992.
10 J. Wang, S. Yin, M. Komatsu, Q. Zhang, F. Saito and T. Sato, Mechanochemical synthesis and photocatalytic activity of nitrogen doped $SrTiO_3$, *J. Ceram. Soc. Jpn.*, 2004, **5**, S1408.
11 C. Zhang, Y. Z. Jia, Y. Jing, Y. Yao, J. Ma and J. H. Sun, Effect of non-metal elements (B, C, N, F, P, S) mono-doping as anions on electronic structure of $SrTiO_3$, *Comput. Mater. Sci.*, 2013, **79**, 69.

12 U. Sulaeman, S. Yin and T. Sato, Visible light photocatalytic properties of Ta and N codoped $SrTiO_3$ nanoparticles, *Int. J. Opt.*, 2010, **2010**, 261420.
13 W. J. Shi and S. Xiong, Ab initio study on band-gap narrowing in $SrTiO_3$ with Nb–C–Nb codoping, *Phys. Rev. B: Condens. Matter Mater. Phys.*, 2011, **84**, 205210.
14 H. Liu, H. Dong and F. Wu, First-principles study on strontium titanate for visible light photocatalysis, *Chem. Phys. Lett.*, 2013, **555**, 141.
15 J. Wang, H. Li, S. Yin and T. Sato, Synthesis of La/N co-doped $SrTiO_3$ using polymerized complex method for visible light photocatalysis, *Solid State Sci.*, 2009, **11**, 182.
16 C. Zhang, Y. Z. Jia, Y. Jing, Y. Yao, J. Ma and J. H. Sun, DFT study on electronic structure and optical properties of N-doped, S-doped, and N/S co-doped $SrTiO_3$, *Phys. B*, 2012, **407**, 4649.
17 P. Liu, J. Nisar, B. Pathak and R. Ahuja, Hybrid density functional study on $SrTiO_3$ for visible light photocatalysis, *Int. J. Hydrogen Energy*, 2012, **37**, 11611.
18 W. Wei, Y. Dai, M. Guo, L. Yu and B. B. Huang, Density functional characterization of the electronic structure and optical properties of N-doped, La-doped, and N/La-codoped $SrTiO_3$, *J. Phys. Chem. C*, 2009, **113**, 15046.
19 C. Wang, H. Qiu, T. Inoue and Q. Yao, Highly active $SrTiO_3$, for visible light photocatalysis: a first-principles prediction, *Solid State Commun.*, 2014, **181**, 5–8.
20 J. A. Dawson, X. Li, C. L. Freeman, J. H. Harding and D. C. Sinclair, The application of a new potential model to the rare-earth doping of $SrTiO_3$ and $CaTiO_3$, *J. Mater. Chem. C*, 2013, **8**, 1574–1582.
21 A. W. Xu, G. Yuan and H. Q. Liu, The preparation, characterization, and their photocatalytic activities of rare earth doped TiO_2, nanoparticles, *J. Catal.*, 2002, **207**, 151–157.
22 N. Aman, P. K. Satapathy, T. Mishra, M. Mahato and N. N. Das, Synthesis and photocatalytic activity of mesoporous cerium doped TiO_2 as visible light sensitive photocatalyst, *Mater. Res. Bull.*, 2012, **47**, 179–183.
23 R. M. Mohamed and I. A. Mkhalid, The effect of rare earth dopants on the structure, surface texture and photocatalytic properties of TiO_2–SiO_2, prepared by sol–gel method, *J. Alloys Compd.*, 2010, **501**, 143–147.
24 H. Shi, T. Zhang, T. An, B. Li and X. Wang, Enhancement of photocatalytic activity of nano-scale TiO_2, particles co-doped by rare earth elements and heteropolyacids, *J. Colloid Interface Sci.*, 2012, **380**, 121–127.
25 P. C. Ricci, A. G. Lehmann, F. Congiu, F. Spadavecchia and C. M. Carbonaro, Structure and photoluminescence of TiO_2 nanocrystals doped and co-doped with N and rare earths (Y^{3+}, Pr^{3+}), *J. Alloys Compd.*, 2013, **561**, 109–113.
26 C. Zhang, Y. Jia, Y. Jing and Y. Yao, New insights into assessing the favorable co-doping dopants with various co-doped cases for the band gap engineering of $SrTiO_3$, *Int. J. Hydrogen Energy*, 2015, **40**, 1343–1351.
27 M. D. Segall, J. D. Lindan Philip, M. J. Probert, C. J. Pickard, P. J. Hasnip, S. J. Clark and M. C. Payne, First-principles simulation: ideas, illustrations and the CASTEP code, *J. Phys.: Condens. Matter*, 2002, **14**, 2717.
28 J. P. Perdew, J. A. Chevary, S. H. Vosko, K. A. Jackson, M. R. Pederson, D. J. Singh and C. Fiolhais, Atoms, molecules, solids, and surfaces: applications of the generalized gradient approximation for exchange and correlation, *Phys. Rev. B: Condens. Matter Mater. Phys.*, 1992, **46**, 6671.
29 D. Vanderbilt, Soft self-consistent pseudopotentials in a generalized eigenvalue formalism, *Phys. Rev. B: Condens. Matter Mater. Phys.*, 1990, **41**, 7892.
30 H. J. Monkhorst and J. D. Pack, On special points for brillouin zone integrations, *Phys. Rev. B: Solid State*, 1976, **13**, 5188.
31 M. C. Qian, W. Y. Hu, Q. Q. Zheng and H. Q. Lin, Electronic structure of $PrBa_2Cu_3O_7$ and $YBa_2Cu_3O_7$: a local spin density approximation with the on-site coulomb interaction study, *J. Appl. Phys.*, 1999, **85**, 4765–4767.
32 D. Marel and G. A. Sawatzky, Electron–electron interaction and localization in d and f transition metals, *Phys. Rev. B: Condens. Matter Mater. Phys.*, 1988, **37**, 10674.
33 T. Mitsui, S. Nouma and B. Landolt, *Numerical data and functional relation in science and technology: crystal and solid state Physics, New Series, Group 2I*, Springer, Berlin, 1982.
34 R. G. Hirst, A. J. King and F. A. Kanda, The barium–strontium equilibrium system, *J. Phys. Chem.*, 1956, **60**, 302–304.
35 S. F. Glavatskikh and A. I. Gorshkov, Natural analog of alpha-titanium in the exhalation products of the great tolbachik fissure eruption (kamchatka), *Dokl. Akad. Nauk*, 1992, **327**, 123–127.
36 R. W. G. Wyckoff, *Crystal Structures*, Interscience Publishers, New York, 2nd edn, 1963.
37 J. Lv, T. Kako and Z. Zou, Band structure design and photocatalytic activity of In_2O_3/N–$InNbO_4$ composite, *Appl. Phys. Lett.*, 2009, **95**, 032107.
38 L. J. Bartolotti, *Absolute electronegativities as determined from Kohn–Sham theory*, Springer, Berlin, Heidelberg, 1987, pp. 27–40.
39 J. Feng, B. Xiao and J. C. Chen, Optical properties of new photovoltaic materials: $AgCuO_2$ and $Ag_2Cu_2O_3$, *Solid State Commun.*, 2009, **149**, 1569.